Journal of Power Sources 195 (2010) 3996–4001

Contents lists available at ScienceDirect

Journal of Power Sources

journal homepage: www.elsevier.com/locate/jpowsour

Direct utilization of methanol and ethanol in solid oxide fuel cells using Cu–Co(Ru)/$Zr_{0.35}Ce_{0.65}O_{2-\delta}$ anodes

Massimiliano Cimenti, Josephine M. Hill*

Department of Chemical and Petroleum Engineering, Schulich School of Engineering, University of Calgary, 2500 University Dr. NW, Calgary, AB T2N 1N4, Canada

ARTICLE INFO

Article history:
Received 27 October 2009
Received in revised form
23 December 2009
Accepted 29 December 2009
Available online 13 January 2010

Keywords:
Solid oxide fuel cells
Direct utilization
Methanol
Ethanol
Zirconia-doped ceria
Copper–cobalt

ABSTRACT

The direct utilization of methanol (MeOH) and ethanol (EtOH) was investigated on Cu–Co(Ru)/$Zr_{0.35}Ce_{0.65}O_2$ anodes for solid oxide fuel cells (SOFC) prepared by impregnation. Cells had similar performance and stability in H_2 and MeOH, while in EtOH the performance varied with time; that is, the power density initially increased, and then declined exponentially. This behavior was likely a consequence of carbon deposition that initially improved electronic conductivity to the anode functional layer, and subsequently blocked active sites. For all cells, the performance was recovered by re-exposing the anode to humidified hydrogen. In some cases, the cell performance exceeded the initial activity measured in hydrogen. Thus, the direct utilization of MeOH and EtOH did not irreversibly deactivate the Co(Ru)/$Zr_{0.35}Ce_{0.65}O_2$ anodes.

1. Introduction

Solid oxide fuel cells (SOFC) convert the chemical energy in a fuel directly into electricity by an electrochemical process [1]. SOFC operate at high temperatures (>700 °C) allowing the highest fuel versatility among all fuel cell types. Examples of future applications for SOFC are stationary energy conversion devices such as combined heat and power generators and auxiliary power units. One of the key components in SOFC is the cathode |electrolyte| anode assembly. Typically, the electrolyte consists of yttria-stabilized zirconia (YSZ), an oxygen-ion conductor; the cathode, where the reduction of oxygen takes place, is typically composed of strontium-doped lanthanum manganite (LSM); and the anode, where the oxidation of the fuel occurs, is typically a composite of nickel and of the electrolyte (Ni/YSZ). Properties such as high ionic and electronic conductivity, sufficient mechanical and chemical stability are of crucial importance for SOFC electrodes. Currently, there is interest in developing SOFC for small portable power generation [2] (<10 kW), in which case it is desirable to directly use liquid fuels rather than H_2. Fuels such as methanol (MeOH) and ethanol (EtOH) [3], which are cheap, easy to store [2], and can be produced by renewable sources [4–7], are the best candidates for small portable SOFC operating in the direct utilization mode [7]. The direct utilization of hydrocarbons or alcohols in SOFC implies that the fuel is added directly to the anode without any preliminary reforming treatment and without the addition of oxidants to achieve internal reforming. The direct utilization of alcohols is challenging on traditional Ni/YSZ anodes because of the irreversible deactivation caused by coking. Thus, the development of alternative anodes characterized by adequate electrochemical activity and stability/resilience to coking is necessary [7,8].

The direct utilization of MeOH and EtOH has been tested on a few anodic materials, such as anode-supported Ni/YSZ [9], Ni/GDC [10], $LaCoO_{3-\delta}$ [11], slurry-painted Cu/$Gd_{0.1}Ce_{0.9}O_{2-\delta}$ [12], impregnated Cu/CeO_2 [13], impregnated Cu/CeO_2 + ZrO_2(0.1)–Sc_2O_3(0.9) [14] and Fe–Ni/ZrO_2(0.1)–Sc_2O_3(0.9) [15]. An extensive study of the direct utilization of MeOH and EtOH on Me/CeO_2 (where Me = Ni, Cu, and Cu–Co), Ni/$Zr_{0.35}Ce_{0.65}O_{2-\delta}$ (ZDC), Cu/ZDC, $La_{0.7}Sr_{0.3}Cr_{0.5}Mn_{0.5}O_{3-\delta}$, $La_{0.7}Sr_{0.3}VO_{3-\delta}$, and $Sr_{0.86}Y_{0.08}TiO_3$ anodes was conducted by the authors of the present study [16–18]. In summary, while Ni and Fe-containing anodes were unstable because of coking and the subsequent irreversible delaminating of the electrode, ceria-based anodes showed better coking-stability but lower performance and, in the case of MeOH [13], redox instability.

Gorte and Vohs' group [19–21] was the first to investigate impregnated Cu–Co/ceria anodes for the direct utilization of methane; this composition exhibited satisfactory performance and promising coking-stability. The primary purpose of the present

* Corresponding author. Tel.: +1 403 210 9488/9589; fax: +1 403 284 4852.
E-mail addresses: max.cimenti@afcc-auto.com (M. Cimenti), jhill@ucalgary.ca (J.M. Hill).

0378-7753/$ – see front matter © 2010 Elsevier B.V. All rights reserved.
doi:10.1016/j.jpowsour.2009.12.122

study was to test the performance and stability of modified Cu–Co/ceria anodes, specifically Cu–Co(Ru)/$Zr_{0.35}Ce_{0.65}O_{2-\delta}$, for the direct utilization of MeOH and EtOH. $Zr_{0.35}Ce_{0.65}O_{2-\delta}$ (ZDC) was considered because of its improved thermal-stability, better compatibility with the electrolyte, and improved oxygen-ion conductivity [22,23] when compared to undoped ceria. Small quantities (<0.5 wt.%) of ruthenium (Ru) were added to improve the catalytic activity of the conductive layer, since Ru/CeO_2 has shown excellent properties for the reforming of EtOH [24,25]. In this study, we focused on the stability and reversibility of Cu–Co(Ru)/ZDC anodes after coking.

2. Experimental

2.1. Preparation

Cells with Cu–Co(Ru)/ZDC anodes were prepared by impregnation of a YSZ porous layer, *ca.* 70 μm thick, supporting a dense YSZ layer (electrolyte), *ca.* 50 μm thick. Porous and dense layers were obtained by tape casting, while LSM cathodes (Praxair Specialty Ceramics), *ca.* 30 μm, were screen-printed as described elsewhere [18]. Cu–Co(Ru)/ZDC anodes were obtained as follows. $Zr_{0.35}Ce_{0.65}O_2$ (ZDC) was deposited on the porous YSZ layer using an aqueous solution of $ZrO(NO_3)_2{\cdot}xH_2O$ and $(NH_4)_2Ce(NO_3)_6$ (Alfa Aesar) at the calculated molar ratio. Impregnated cells were fired at 723 K [18], and the impregnation procedure was repeated until the weight of ZDC was equivalent to approximately 30 wt.% of the YSZ porous layer. Cu–Co was deposited using a saturated solution containing 64.2 wt.% $Cu(NO_3)_2{\cdot}3H_2O$ and 35.8 wt.% $Co(NO_3)_2{\cdot}6H_2O$ (99.99% metal basis, Alfa Aesar) in isopropyl alcohol (IPA), which is equivalent to a weight ratio of 7/3 of reduced Cu and Co, as recommended by others [20,21]. The procedure was repeated until the metal loading was approximately 40 wt.%. The impregnation of Ru was done in a single step using a 40 g L^{-1} solution of $RuCl_3$ (Alfa Aesar) in IPA, followed by calcination at 1073 K for 1 h. The Ru content was estimated to be <0.5 wt.% with respect to the metal loading. Prepared cells were assembled in the experimental set-up described in detail elsewhere [18].

2.2. Testing

The characteristic performance and stability of cells with Cu–Co(Ru)/ZDC anodes was tested in H_2, MeOH, and EtOH at 1073 K. Performance was determined by measuring the steady-state polarization (*i–V* curve) and electrochemical impedance spectroscopy (EIS). Stability was determined by monitoring the current produced during a potentiostatic step of 20 h, or by comparing polarization curves obtained before and after exposure to either alcohol. Electrochemical measurements were done using a standard electrochemical interface (1287 Potentiostat + 1260 FRA, Solartron Analytical, U.K.). Experiments were run in triplicate for each alcohol type (Cells 1–3 in MeOH; Cells 4–6 in EtOH). The typical testing protocol was as follows. First, cells were tested in humidified H_2 (~3 vol.% H_2O) for at least 24 h. Then, the feed was switched to pure alcohol (MeOH or EtOH) that was injected directly to the anode compartment using a syringe pump at 2 mL h^{-1} (equivalent to 1.37E−5 and 9.51E−6 mol s^{-1} of MeOH and EtOH, respectively). After 24 h with an alcohol feed, cells were re-exposed to humidified H_2 to test the performance-reversibility after coking. One of the three cells tested with each alcohol was not re-exposed to H_2 and the carbon deposits were characterized. During testing the composition of the outlet gases was measured by gas-chromatography (mGC 3000 Agilent Technologies, U.S.A.) [18,26].

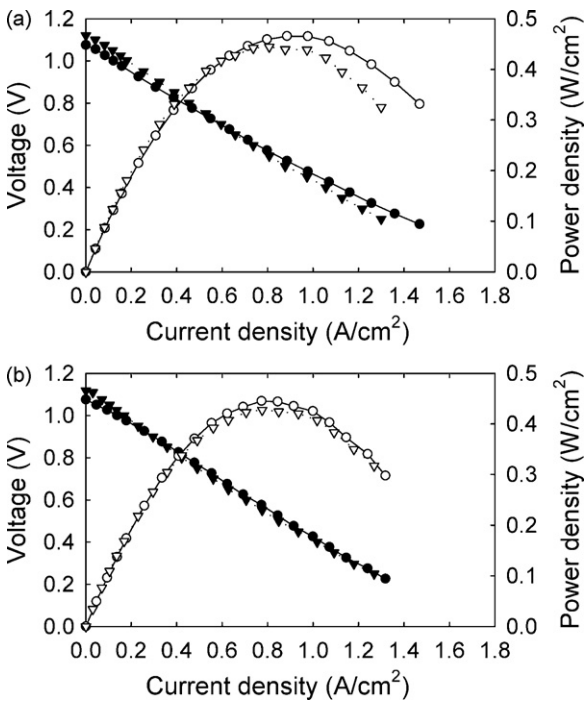

Fig. 1. Initial (a) and final (b) polarization curves (filled symbols) and power density (open symbols) for Cell 1 at 1073 K in humidified H_2 (●, ○) and in pure MeOH (▼, ▽).

2.3. Post-testing characterization

Tested cells were analyzed by electron microscopy (SEM) and energy dispersive X-ray spectroscopy (EDX) using a XL30 environmental scanning electron microscope (Philips). Carbon deposits were analyzed by Temperature-Programmed Oxidation (TPO) by heating the sample at 10 K min^{-1} in 10% O_2 in He and monitoring the exhaust gases with a mass spectrometer [27].

3. Results and discussion

3.1. Performance and stability in MeOH

A representative example of the polarization curves obtained using Cu–Co(Ru)/ZDC anodes in H_2 and MeOH at 1073 K is shown in Fig. 1. The curves in Fig. 1a were obtained at the start of exposure to either H_2 or MeOH, while the curves in Fig. 1b were obtained after the cell had been exposed to MeOH for 24 h. The open circuit potential (OCP) in humidified H_2 for Cell 1 was 1.075 V, which is less than 10 mV lower than the theoretical value for the testing conditions, indicating that the cell was sealed well. In MeOH, the average OCP was 1.120 V but noisy (±15 mV). The average composition of the outlet gases from the cell was 48 vol.% H_2, 25% CO, 2% HCHO, and 24% of unreacted MeOH. The concentration of CO_2, H_2O, and CH_4 was <1%. The theoretical OCP for this composition and conditions is 1.250 V. The difference between measured and theoretical OCP suggests that the local composition at the functional layer may be different from the outlet; thus, there could be concentration gradients through the electrode thickness. The maximum power densities obtained for this specific cell were 0.465 and 0.444 W cm^{-2} in humidified H_2 and pure MeOH, respectively. The maximum fuel utilization during stability testing was 1.6%, which implies that coking was favorable as predicted by theoretical calculations presented elsewhere [17].

The impedance spectra measured in H_2 and MeOH for Cell 1 are shown in Fig. 2. In H_2, the spectrum is composed by a main

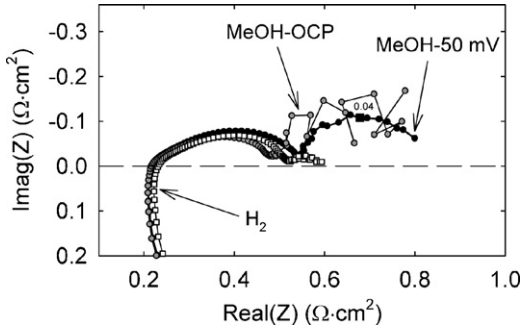

Fig. 2. Impedance spectra for Cell 1 at 1073 K in H_2 (white) and pure MeOH at OCP (gray) and 50 mV bias (black). The square marker corresponds to the frequencies (in Hz) labeled.

depressed arc and by a smaller low-frequency arc (~0.06 Ω cm^2 with peak frequency at 0.1 Hz). The main arc can be attributed to charge-transfer reactions (mainly H_2 and CO oxidation) combined with the effect of the ionic conductivity of the ZDC phase [28], while the smaller arc could be an example of gas-diffusion [29] and gas-conversion impedance [30]. However the peak-frequencies for gas-diffusion or gas-conversion impedance estimated according to Primdahl and Mogensen [29,30] are at least one order of magnitude higher, thus the contribution of these processes is likely convoluted within the main impedance arc. The low-frequency arc could be caused by diffusion through the porous anode, as the microstructure of these anodes was not optimized. In MeOH, the low-frequency arc was larger than in H_2. At OCP this part of the spectrum was noisy, while after applying a small overpotential (*e.g.* 50 mV in Fig. 2) the impedance signal was cleaner showing a low-frequency arc of ~0.25 Ω cm^2. As for H_2, this feature could be related to diffusion in the anode pores and/or to the decomposition of MeOH. The catalytic decomposition of MeOH on the anode surface generates up to 3 mol of products per mole of MeOH reacted, causing a convective flow from the anode surface that will hinder the diffusion of reactants to the active layer. Thus, the catalytic decomposition of MeOH could be the origin of the characteristic low-frequency arc observed.

Cells 1 and 2 were tested for 24 h in H_2, then for 24 h in MeOH, and then again in H_2. The stability measured in MeOH was similar to that observed in H_2. The average deactivation during the 20 h at constant voltage (0.6 V) was 0.2 Ω cm^2. Cell performances in MeOH before and after stability tests are shown in Fig. 1a and b, respectively. The polarization curve of the cell re-exposed to H_2 is also shown in Fig. 1b. The performances for the three cells tested in MeOH are summarized in Fig. 3. Note, Cell 3 was used for the TPO analysis and so was not exposed to humidified H_2 after MeOH. The variability (±15%) in performance between samples could be a result of the preparation procedure, which involves sequential impregnations. Nevertheless, the trends summarized in Fig. 3 are

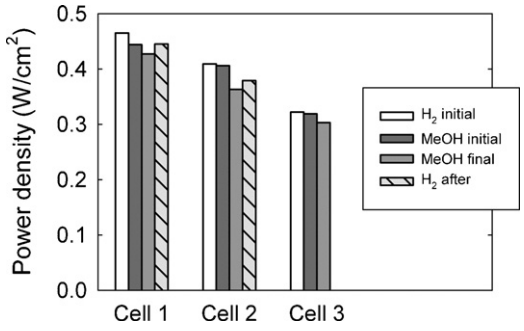

Fig. 3. Maximum power densities obtained for the cells tested in MeOH.

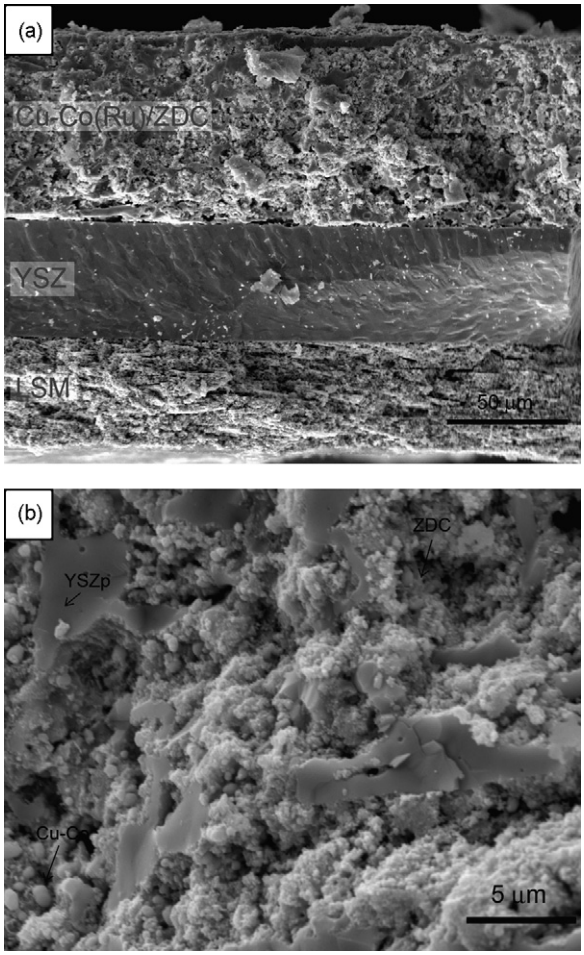

Fig. 4. SEM micrographs of a Cu–Co(Ru)/ZDC anode tested in MeOH: (a) anode cross-section; (b) close-up of an anode pore in the cross-section. Segregated phases (*i.e.* YSZ, ZDC, and metal) detected by EDX are indicated and labeled.

in agreement for the stability and resilience to coking. That is, the power densities of the cells in MeOH were initially similar to that in H_2, deactivated over time, but then some if not all of the activity could be recovered by exposure to humidified H_2.

The morphology of tested anodes is shown in the SEM micrographs of Fig. 4. There was no delaminating or dusting of the anode structure after exposure to MeOH, which is a characteristic problem for Ni-containing anodes [26,31]. Tested anodes appeared to be clean from carbon deposits after visual inspection; however, carbon was detected by EDX throughout the cross-section and on the anode surface. The measurement of coke distribution (semi-qualitative) through the electrode thickness was attempted by EDX spot-analysis, but no concentration trend was observed, indicating that the decomposition of MeOH is likely to occur on the entire anode.

TPO profiles (not shown) of Cell 3 after testing in MeOH were characterized by three temperature peaks at approximately 510 K (smaller), 675 K (medium), and 890 K (larger), which implies the presence of different types of carbon. The carbon types could not be distinguished in the SEM analysis.

3.2. Performance and stability in EtOH

A representative example of polarization curves obtained using Cu–Co(Ru)/ZDC anodes in H_2 and EtOH at 1073 K is shown in Fig. 5. The initial OCP and maximum power density in humidified H_2 for Cell 4 was 1.063 V and 0.496 W cm^{-2}, respectively. In pure EtOH, the

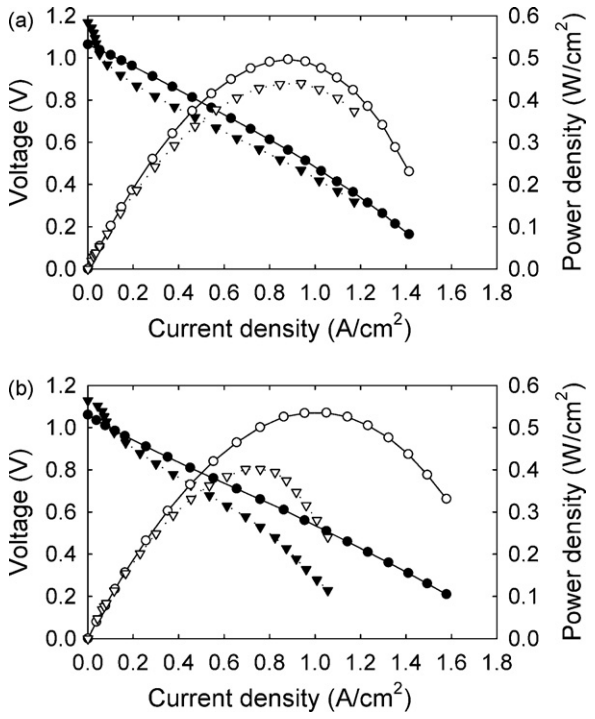

Fig. 5. Initial (a) and final (b) polarization curves (filled symbols) and power density (open symbols) for Cell 4 at 1073 K in humidified H_2 (●, ○) and in pure EtOH (▼, ▽).

OCP and maximum power density were 1.168 V and 0.440 W cm^{-2}. Given these performances, the fuel utilization was always <1.9%, which is well within the carbon formation region [17]. The outlet gas from the cell was composed of CH_4 (25%), CO (25%), H_2 (20%), H_2O (15%), C_2H_4 (5%), CO_2 (4%), and traces (<1%) of C_2H_6 and CH_3CHO. The theoretical OCP for this composition is ~50 mV lower than the measured OCP, indicating that the gas composition at the anode interface was likely closer to equilibrium composition for the reaction of EtOH decomposition [17] (*i.e.* higher in H_2 and CO, and lower in H_2O and CO_2) than the gas composition measured at the outlet. EtOH can decompose in the gas phase (pyrolysis) as well over the anode surface (catalytic decomposition). Pyrolysis is kinetically limited [31]. In the low overpotential region (1.1–1.0 V in Fig. 5), the steady-state polarization curve was not linear. This behavior could be a result of the presence of oxygen ions which migrated from the cathode, influencing the reaction of EtOH decomposition, or could be related to the electrochemical oxidation of decomposition products other than H_2 and CO.

The characteristic stability profile of Cu–Co(Ru)/ZDC anodes in EtOH is shown in Fig. 6. Although the initial power densities

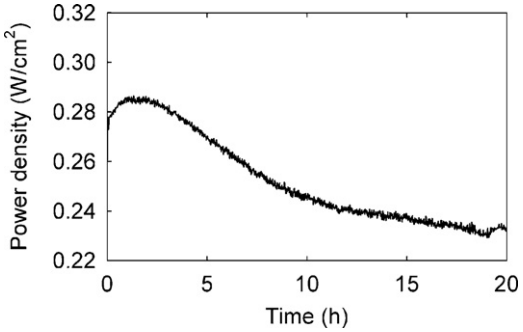

Fig. 6. Stability at 1073 K and 0.6 V in pure EtOH for Cell 6.

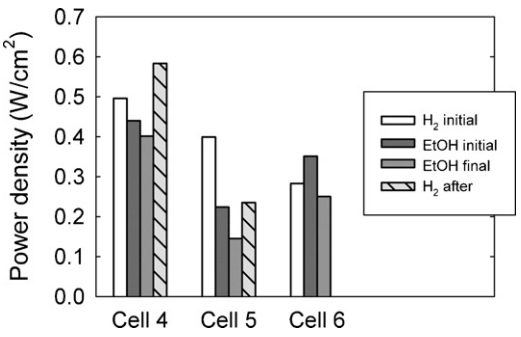

Fig. 7. Maximum power densities obtained for the cells tested in EtOH.

varied, all cells tested had a similar behavior. Specifically, the performance initially increased, then peaked after approximately 2 h, and finally decreased exponentially. Cu–Co(Ru)/ZDC anodes deactivated slower than all other anode-materials that we have tested [16]. The final OCP in pure EtOH for Cell 4 after 20 h of direct utilization was 1.130 V (Fig. 5b, compared to 1.168 V in Fig. 5a), which is closer to the theoretical value corresponding to the outlet gas composition (1.118 V) than to the OCP for the equilibrium composition. If the active sites on the anode surface are blocked by carbon deposits, the catalytic decomposition of EtOH will be hindered and the equilibrium gas-phase composition will not be reached. The final power density in EtOH was 0.401 W cm^{-2}. Performance results for all cells tested in EtOH are summarized in Fig. 7. As for cells tested in MeOH, there was variability in the performance (±20%) between samples. Cell 6, for example, showed higher initial performance in EtOH than in H_2, while for the other cells the performance in EtOH was lower. Cells 4 and 5 showed improved performance after re-exposure to H_2. This behavior was possibly related to the improvement of the electronic conductivity from the formation of carbon deposits [32].

The area-specific impedance spectra measured in H_2 and EtOH for Cell 4 are shown in Fig. 8. The spectra obtained in H_2 were similar to those described above for MeOH; while in EtOH, the spectrum was characterized by a low-frequency capacitive tail similar to that described in an earlier study on Cu(Ru)/ZDC anodes [18]. The impedance spectra of Cell 4 in humidified H_2 at various times after 24 h of exposure to pure EtOH are shown in Fig. 9. A characteristic behavior was observed: immediately after the cell was re-exposed to H_2 the impedance spectrum still had a low-frequency capacitive arc as in EtOH (compare the spectra taken after 20 min in H_2 in Fig. 9 and in EtOH in Fig. 8). As time passed the arc closed towards the real-axis and its diameter decreased exponentially with time up to 12 h in H_2, after which the impedance spectra were stable; the size of the low-frequency

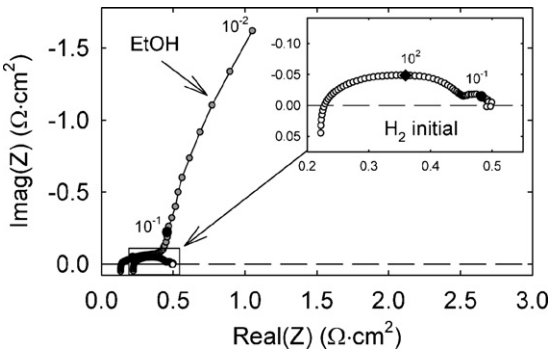

Fig. 8. Impedance spectra for Cell 4 at 1073 K in H_2 (white) and in pure EtOH at OCP (gray). Markers correspond to the frequencies (in Hz) labeled.

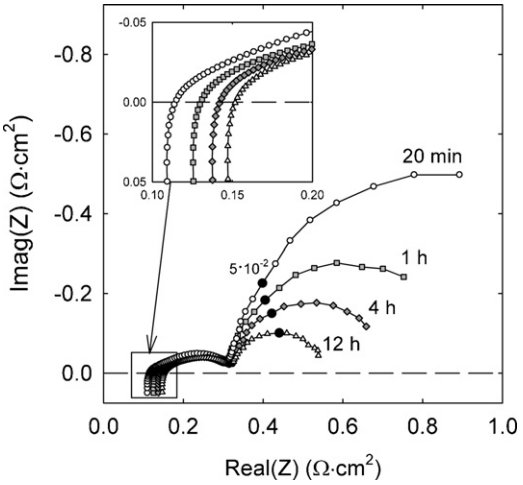

Fig. 9. Equilibrium impedance and expanded view of the high-frequency intercepts (inset) for Cell 4 after 20 min (○), 1 h (□), 4 h (◊), and 12 h (△) of re-exposure to H_2 at 1073 K after 24 h in pure EtOH. Markers correspond to the frequencies (in Hz) labeled.

arc was ~0.2 Ω cm^2, and the average peak-frequency was ~0.03 Hz. The high-frequency intercept (R_Ω), which represents the ohmic resistance of the cell (*i.e.* electrolyte + electron-conducting portion of the anode + current collectors), also changed with time, increasing from 0.102 to 0.140 Ω cm^2, as shown in the inset of Fig. 9.

A loose and thin layer (~1/2 mm) of black carbon deposits (possibly soot) was visible on all anodes tested in EtOH. This layer was cleaned off before SEM analysis. In general the anode microstructure examined by SEM did not appear to be damaged by coking (Fig. 10a), and the pores in the anode cross-section did not appear to be plugged with coke, even though carbon was always detected by EDX (Fig. 10b). Amorphous carbon was found on the anode surface (Fig. 10c), and carbon fibers were also found in isolated areas (Fig. 10d), which could be caused by the presence of Co [31].

The presence of larger amounts of carbon on the anode surface provides a possible explanation to the impedance results obtained in H_2 after exposure to EtOH (Fig. 9). If we assume that the low-frequency arc was caused by diffusion only, given the peak-frequency it is possible to calculate a value for the effective diffusivity [29]. Assuming also that the thickness of the diffusion layer is equal to the thickness of the anode, the effective diffusivity is ~1E−5 cm^2 s^{-1}, which is more than 5 orders of magnitude smaller than the binary diffusion coefficient for H_2 and H_2O at 1073 K (7.47 cm^2 s^{-1}). Therefore, the low-frequency arc observed cannot be attributed to gas-diffusion through a stagnant layer, but could be caused by Knudsen diffusion through a porous layer.

The passage of H_2 molecules through the electrode pores would be considerably hindered if the pores were partially filled with coke. Assuming that after impregnation the electrode had a residual porosity of ~1%, it is possible to estimate the maximum diameter of the pores that would give an effective diffusivity as calculated for this case [33]. For a peak-frequency of 0.05 Hz and for an electrode thickness of 100 μm, the estimated pore diameter is ~5 nm. However, SEM analysis indicates that the pores were larger. Also assuming that most of the mass-transfer limitations happened on the surface of the anode, which, as shown in Fig. 10c, was always covered by a thick layer of carbon, leads to an inconsistency because the limiting current predicted for the effective diffusivity corresponding to the low-frequency arc is lower than the maximum

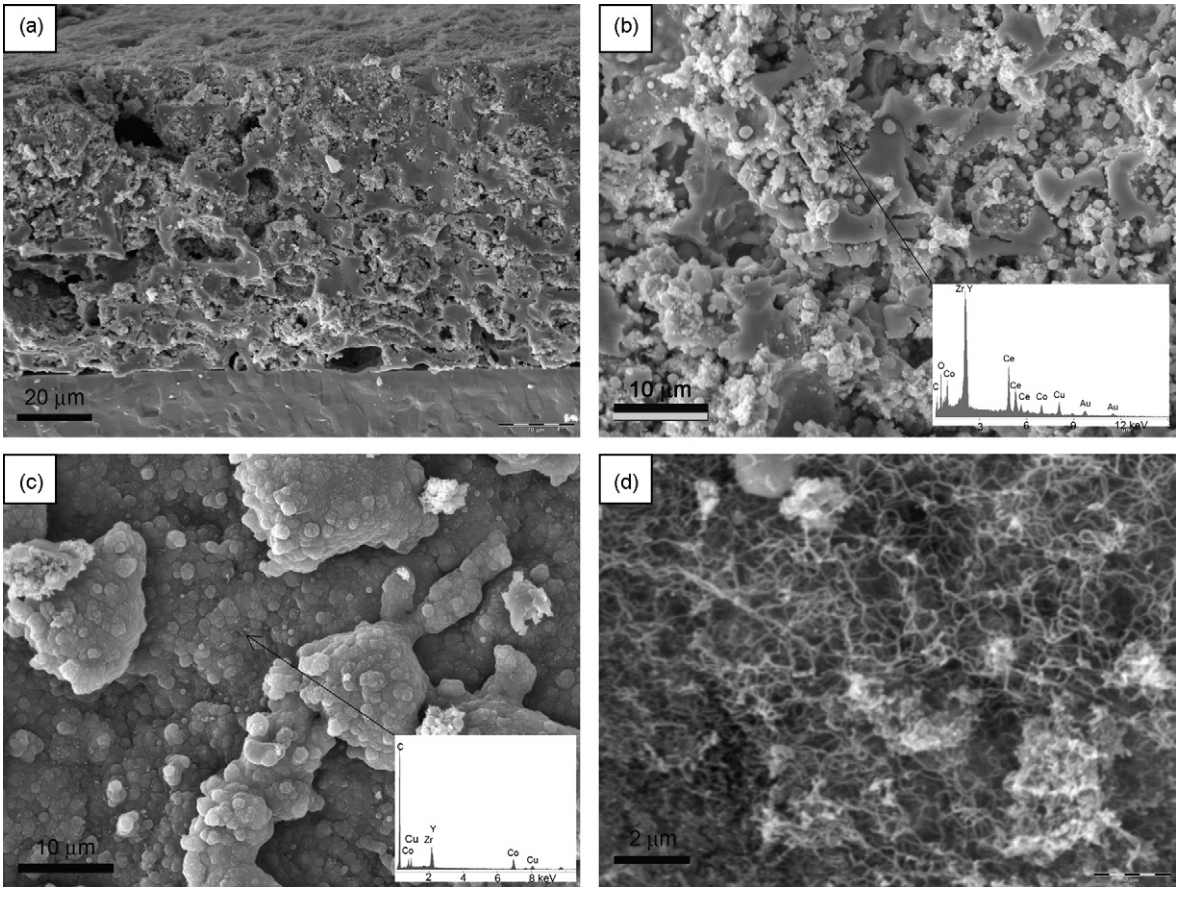

Fig. 10. SEM micrographs of a Cu–Co(Ru)/ZDC anode tested in EtOH: (a) anode cross-section; (b) close-up of a pore with EDX profile.; (c) surface of the electrode covered by dense carbon deposits; (d) fibrous carbon deposits found in isolated spots of the anode surface.

current obtained (Fig. 5b). Finally, the characteristic impedance reported in Fig. 9 could be related to the pore size distribution and tortuosity of coked anodes (that was not determined) and to the process of partial removal of carbon deposits from the smaller pores on exposure to humidified H_2.

TPO profiles (not shown) of carbon deposits on Cell 6 tested in EtOH were characterized by three peaks at 510 K (smaller), 710 K (medium), and 850 K (larger), similar to the TPO profiles of Cell 3 tested in MeOH. The intensity of the CO_2 signal, however, was higher and the relative heights of the three peaks were different, with the peak at 850 K being significantly higher for Cell 6. As for MeOH, the carbon was relatively weakly bonded and could be removed by exposure to humidified H_2 at 1073 K as discussed above.

4. Conclusions

The direct utilization of MeOH and EtOH was tested on Cu–Co(Ru)/ZDC anodes at 1073 K. Cell performances in pure MeOH were only slightly inferior to that measured in humidified H_2, the performance degradation was very similar to that observed in pure H_2 and little coke was deposited after 24 h of exposure. Impedance spectra obtained in MeOH were characterized by a short capacitive tail at the low frequencies that could be related to the catalytic decomposition of MeOH on the anode surface. Coking was more severe during the direct utilization of EtOH and cells were less stable. During stability testing, cells exhibited a characteristic trend of activation–deactivation with time that can be explained by the simultaneous improvement of electronic conductivity [32] and degradation of mass transfer caused by carbon deposits within the pores [18]. Cu–Co(Ru)/ZDC anodes were not irreversibly deactivated by coking, as performance was recoverable with exposure to humidified H_2.

Acknowledgments

This work was financed with a Natural Sciences and Engineering Research Council (NSERC) grant. M.C. is grateful to NSERC and Killam Trust for financial support.

References

[1] S.C. Singhal, K.E. Kendall, High Temperature Solid Oxide Fuel Cells—Fundamentals, Design and Applications, 1st ed., Elsevier Ltd., Oxford, UK, 2003.
[2] S.C. Singhal, Solid State Ionics 152 (2002) 405–410.
[3] K. Sasaki, K. Watanabe, K. Shiosaki, K. Susuki, Y. Teraoka, J. Electroceram. 13 (2004) 669–675.
[4] G.A. Olah, Beyond Oil and Gas: The Methanol Economy, Wiley-VCH, Weinheim, Germany, 2006.
[5] K. Sasaki, H. Kojo, Y. Hori, R. Kikuchi, K. Eguchi, Electrochemistry 70 (2002) 18–22.
[6] K. Sasaki, K. Watanabe, Y. Teraoka, J. Electrochem. Soc. 151 (2004) A965–A970.
[7] M. Cimenti, J.M. Hill, Energies 2 (2009) 377–410.
[8] A. Atkinson, S. Barnett, R.J. Gorte, J.T.S. Irvine, A.J. McEvoy, M. Mogensen, S.C. Singhal, J. Vohs, Nat. Mater. 3 (2004) 17–27.
[9] Y. Jiang, A.V. Virkar, J. Electrochem. Soc. 148 (2001) A706–A709.
[10] R. Muccillo, E.N.S. Muccillo, F.C. Fonseca, D.Z. de Florio, J. Electrochem. Soc. 155 (2008) B232–B235.
[11] N. Sammes, L. Varadaraj, Denki Kagaku 63 (1995) 41–46.
[12] D.J.L. Brett, A. Atkinson, D. Cumming, E. Ramirez-Cabrera, R. Rudkin, N.P. Brandon, Chem. Eng. Sci. 60 (2005) 5649–5662.
[13] T. Kim, K. Ahn, J.M. Vohs, R.J. Gorte, J. Power Sources 164 (2007) 42–48.
[14] X.F. Ye, B. Huang, S.R. Wang, Z.R. Wang, L. Xiong, T.L. Wen, J. Power Sources 164 (2007) 203–209.
[15] B. Huang, S.R. Wang, R.Z. Liu, T.L. Wen, J. Power Sources 167 (2007) 288–294.
[16] M. Cimenti, Direct Utilization of Methanol and Ethanol in Solid Oxide Fuel Cells, Ph.D. Thesis, University of Calgary, Calgary (Canada), Calgary, 2008.
[17] M. Cimenti, J.M. Hill, J. Power Sources 186 (2009) 377–384.
[18] M. Cimenti, J.M. Hill, Asia-Pac. J. Chem. Eng. 4 (2009) 45–54.
[19] M.D. Gross, J.M. Vohs, R.J. Gorte, Electrochim. Acta 52 (2007) 1951–1957.
[20] S.I. Lee, K. Ahn, J.M. Vohs, R.J. Gorte, Solid-State Lett. 8 (2005) A48–A51.
[21] S.I. Lee, J.M. Vohs, R.J. Gorte, J. Electrochem. Soc. 151 (2004) A1319–A1323.
[22] Z. Zhang, Y. Zhang, Z. Mu, P. Yu, X. Ni, S. Wang, L. Zheng, Appl. Catal. B 76 (2007) 335.
[23] M. Sugiura, Catal. Surv. Asia 7 (2003) 77–87.
[24] C.W. Sun, Z. Xie, C.R. Xia, H. Li, L.Q. Chen, Electrochem. Commun. 8 (2006) 833–838.
[25] J. Rass-Hansen, C.H. Christensen, J. Sehested, S. Helveg, J.R. Rostrup-Nielsen, S. Dahl, Green Chem. 9 (2007) 1016–1021.
[26] M. Cimenti, V. Alzate-Restrepo, J.M. Hill, J. Power Sources, in press, doi:10.1016/j.jpowsour.2009.12.119.
[27] V. Alzate-Restrepo, J.M. Hill, Appl. Catal. A 342 (2008) 49.
[28] S.B. Adler, J.A. Lane, B.C.H. Steele, J. Electrochem. Soc. 143 (1996) 3554–3564.
[29] S. Primdahl, M. Mogensen, J. Electrochem. Soc. 146 (1999) 2827–2833.
[30] S. Primdahl, M. Mogensen, J. Electrochem. Soc. 145 (1998) 2431–2438.
[31] M. Cimenti, J.M. Hill, J. Power Sources 195 (2010) 54–61.
[32] S. McIntosh, H.P. He, S.I. Lee, O. Costa-Nunes, V.V. Krishnan, J.M. Vohs, R.J. Gorte, J. Electrochem. Soc. 151 (2004) A604–A608.
[33] E.L. Cussler, Diffusion: Mass Transfer in Fluid Systems, 2nd ed., Cambridge University Press, New York, 1997.